Journal of Engineering Science and Technology
Vol. 12, No. 1 (2017) 214 - 228

MODELLING THE DELAMINATION FAILURE ALONG THE CFRP-CFST BEAM INTERACTION SURFACE USING DIFFERENT FINITE ELEMENT TECHNIQUES

AHMED W. AL-ZAND*, WAN HAMIDON W. BADARUZZAMAN, AZRUL A. MUTALIB, SALAM J. HILO

Department of Civil and Structural Engineering, Universiti Kebangsaan Malaysia, Jalan Reko, 43600 Bangi, Selangor, Malaysia
*Corresponding Author: ahmedzand70@gmail.com

Abstract

Nonlinear finite element (FE) models are prepared to investigate the behaviour of concrete-filled steel tube (CFST) beams strengthened by carbon fibre reinforced polymer (CFRP) sheets. The beams are strengthened from the bottom side only by varied sheet lengths (full and partial beam lengths) and then subjected to ultimate flexural loads. Three surface interaction techniques are used to implement the bonding behaviour between the steel tube and the CFRP sheet, namely, full tie interaction (TI), cohesive element (CE) and cohesive behaviour (CB) techniques using ABAQUS software. Results of the comparison between the FE analysis and existing experimental study confirm that the FE models with the TI technique could be applicable for beams strengthened by CFRP sheets with a full wrapping length; the technique could not accurately implement the CFRP delamination failure, which occurred for beams with a partial wrapping length. Meanwhile, the FE models with the CE and CB techniques are applicable in the implementation of both CFRP failures (rapture and delamination) for both full and partial wrapping lengths, respectively. Where, the ultimate loads' ratios achieved by the FE models using TI, CE and CB techniques about 1.122, 1.047 and 1.045, respectively, comparing to the results of existing experimental tests.

Keywords: ABAQUS, CFST Beam, delamination, CFRP sheets, Finite Element

1. Introduction

Engineers have increasingly recommended and applied concrete-filled steel tube (CFST) members in modern structural projects because this type of structural member has high strength capacity and ductility compared to the conventional

Nomenclatures

E_C	Modulus of elasticity for concrete, GPa
$E_{cfrp.patch}$	Modulus of elasticity of each CFRP patch, GPa
$E_{cfrp.sheet}$	Modulus of elasticity of CFRP sheet, GPa
E_{ad}	Modulus of elasticity of adhesive layer, GPa
f_{cu}	Ultimate cube compressive strength of concrete, MPa
f_{ck}	Characteristic compressive strength of concrete, MPa
f	Concrete compressive strength at relative ε, MPa
f_y	Steel yielding strength, MPa
G_{ad}	Shear modulus of the adhesive material, MPa
G_n	Fracture energy value due to a tension (normal) direction, N/mm
G_s *and* G_t	Fracture energy value due to a shear directions (first and second shear directions), N/mm
G_I	Total interfacial fracture energy required to satisfy the ultimate failure for mode-I (tension direction), N/mm
G_{II}	Total interfacial fracture energy required to satisfy the ultimate failure for mode-II (both shear directions), N/mm
K_n	Elastic stiffness or interfacial stiffness for the tension (normal) direction, MPa
K_s *and* K_t	Elastic stiffness or interfacial stiffness for the shear directions (first and second shear directions), MPa
$t_{cfrp.patch}$	Equivalent thickness of each CFRP patch, mm
$t_{cfrp.sheet}$	Thickness of each layer of CFRP sheet, mm
t_{ad}	Thickness of each adhesive layer, mm
n	Total number of CFRP layers
t_n	Stresses along the tension (normal) direction of the adhesive material, MPa
t_s *and* t_t	Stress along the shear directions of the adhesive material (first and second shear directions), MPa
T_n	Peak value of the tension (normal) strength of the adhesive material, MPa
T_s *and* T_t	Peak values of shear strength of the adhesive material at the first and the second shear directions, MPa

Greek Symbols

σ_{ad}	*Ultimate tensile strength of adhesive layer, MPa*
$\sigma_{cfrp.patch}$	Equivalent ultimate tensile strength for each CFRP patch, MPa
$\sigma_{cfrp.sheet}$	Ultimate tensile strength of CFRP sheet, MPa
ε	*Strain at relative concrete strength (f)*
ε_o	*Strain at ultimate compressive concrete strength (f_{cu})*

structural members. Filling the hollow steel tubes by concrete will delaying and/or preventing the local buckling of tube's plate which usually happened in the high compression zones specifically for the members under flexural loads [1], where the local buckling could be occurred at the supports/mid-span of the beam.

CFST flexural members could require strengthening similar to other structural members for various reasons, such as degradation due to ageing, fatigue and/or upgrade of the existing structures. Carbon fibre reinforced polymer (CFRP) composite materials have become a sufficient solution for strengthening and/or upgrading the steel structural members compared to the conventional strengthening methods. CFRP sheets has high tensile strength and modulus of elasticity compared to the values of steel. This type of composite material has exhibits perfect performance when used to strengthen the existing steel members as presented in several experimental and theoretical studies, as summarized by Zhao and Zhang (2007) [2]. Several studies have examined specifically the effects of surface preparation, shape and length of interactions between steel and CFRP material, in addition to the effects of different types of CFRP and adhesive materials explored, such as done by other researchers [3-7]. The bond delamination failure could be occurred along the CFRP-steel interaction surface when the adhesive layer subjected to flexural stress, where the adhesive layer will be subjected to mixed-mode stresses (tensile and shear) at this case causing the debonding failure even before achieving the CFRP ultimate strength [8-10].

A few studies have investigated the behaviours of hollow/concrete-filled steel tube members strengthened by CFRP material and subjected to the flexural and/or combined loads [11-14]. Recently the numerical analysis using the finite element (FE) software became a typical tool used by researchers for representing several structural case studies, in which the FE models demonstrate perfect results compared to those obtained in experimental works on steel members strengthening by CFRP material, such as presented in [8, 14-17]. Therefore, the main objective of the present study is to employ the FE model to investigate the bonding behaviour along the surface interaction between CFST beam and CFRP sheet, in which the adhesive material between steel and CFRP sheet is implemented through using three different techniques, namely, tie interaction (full bond interaction), independent adhesive layer (cohesive element) and breakable nodes along the surface interaction (cohesive behaviour). The FE models are examined with the existing experimental tests conducted by Sundarraja and Prabhu [14] to evaluate the validity of each interaction technique.

2. Finite Element Modelling

2.1. Description of the model

The loading system and boundary conditions shown in Fig. 1, which adopted to prepare the 3D nonlinear FE model prepared by ABAQUS software to represent the CFST beams strengthened by CFRP sheets from the bottom side only. However, the FE specimen modelling adopts a quarter model using the symmetry parameters technique for all of the beam materials and geometry, which is available in the ABAQUS software programme [18]. The current study performs a quasi-static analysis using the displacement load option at loading points that

are increased gradually at the rate of 0.2 mm/s until the ultimate limit of the beam capacity is reached.

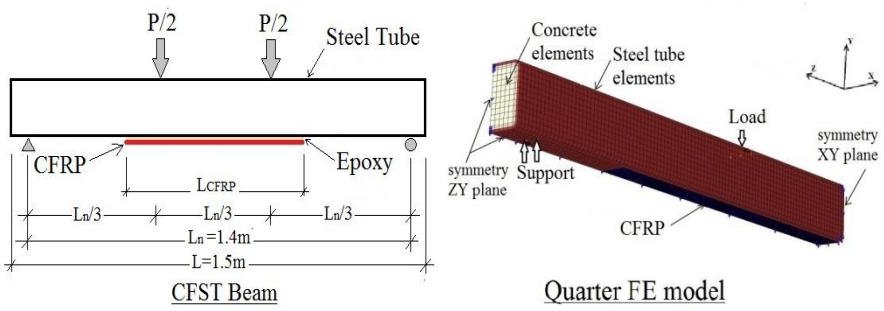

Fig. 1. Boundary conditions and strengthening scenario of the CFST beam.

2.2. Description of elements

The FE software (ABAQUS) has several types of elements in the Element Library-Standard. However, the steel tube modelled with element types C3D8R and C3D8RH is selected for the concrete material, whereas the shell element type S4R is used for the CFRP patch. The element library has a 'cohesive element' type, COH3D8, which is typically used in modelling the adhesive material. This element is applicable for conditions characterized by damage/deform, particularly in the analysis of shear and tensile stresses. The 'cohesive element' technique, which has been used in [16, 19], exhibits excellent results in terms of the implementation of the adhesive behaviour along the surface interaction between the two adherent materials (steel and CFRP).

2.3. Surface interactions

The surface interaction between the beam components of concrete, steel tube, CFRP and adhesive materials is one of the most important parameters in the FE models to verify the experimental results. However, this study adopts three different scenarios/techniques for modelling the adhesive material (i.e., resin epoxy) that is applied along the surface interaction between the steel tube and the CFRP patch. The first scenario uses a full tie interaction (TI) technique; the second scenario provides an independent layer for the adhesive material using the 'cohesive element' (CE) technique; and the third scenario uses the 'cohesive behaviour' (CB) technique that adopts breakable nodes along the surface interaction; all of these techniques are available in the ABAQUS software. Perfect interaction contact between the inner surface of the steel tube and the outer surface of the concrete was used to build the FE models in this study, because of no slip has been recorded/occurred along this interaction surface in the corresponding experimental study [14].

2.4. Material properties

The material properties adopts in this study clarified clearly in these following section to enhance the understanding of the modelling these materials in the FE models.

2.4.1. Steel

The steel tube implemented in the present FE models is a square hollow section (91.5 mm × 91.5 mm × 3.6 mm) with a total length of 1.5 m. The steel properties for Poisson's ratio, modulus of elasticity and yielding strength are 0.3, 204 GPa and 258 MPa, respectively. However, the steel material is an elastic-plastic isotropic material. Therefore, to implement the mechanical properties of steel in the FE models, the elastic-isotropic option is selected to identify the modulus of elasticity and Poisson's ratio. Meanwhile, the plastic-isotropic option is selected to identify the yielding strength and plastic strain values. The well-known J2 flow theory is adopted in this study to implement the plastic behaviour of steel material. Figure 2 shows the tri-linear stress-strain model provided by [20], which the current study adopts to estimate the stress-strain values in the FE models.

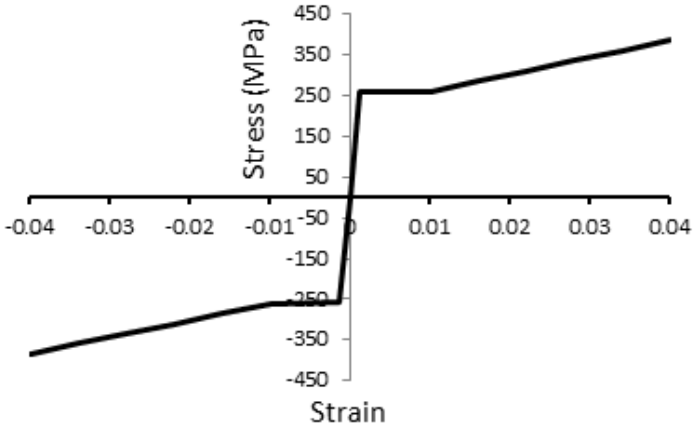

Fig. 2. Stress-strain curve of steel material used in the FE model.

2.4.2. Concrete

The concrete properties adopted in this study are 38.5 MPa and 0.2 for cube compressive strength and Poisson's ratio, respectively. The concrete is an isotropic material that is prone to crushing and cracking at the plastic range. Therefore, for the mechanical-elastic properties, the elastic-isotropic option is selected to identify the modulus of elasticity and Poisson's ratio. Meanwhile, the concrete damaged plasticity option is selected to identify the mechanical-plasticity properties. Figure 3 shows the uniaxial stress-strain relationship of concrete material of concrete, in which the same equations were used by [14] are employed in this study. The Young's modulus was evaluated as per IS 456:2000:

$$E_C = 5000\sqrt{f_{ck}} \tag{1}$$

$$\varepsilon_O = 2\times\left(f_{cu}/E_C\right) \tag{2}$$

$$f = E_C \times \varepsilon / \left(1+\left(\varepsilon/\varepsilon_O\right)^2\right) \tag{3}$$

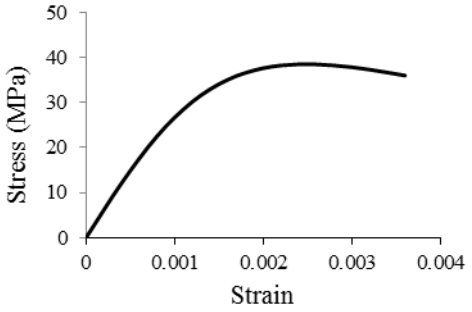

Fig. 3. Uniaxial stress-strain relationship of the concrete material used in the FE model.

2.4.3. CFRP sheet

Unidirectional carbon fibre reinforced polymer (CFRP) sheet is used to strengthen the CFST beams; the type of CFRP sheet is MBrace 240, with modulus of elasticity, ultimate tensile strength, sheet thickness and Poisson's ratio of 240 GPa, 3800 MPa, 0.24 mm and 0.4, respectively. However, the CFRP material is an elastic-brittle material; thus, the mechanical material is modelled as damage for fibre reinforced polymer—Hashin Damage. Moreover, the CFRP material is treated as an orthotropic material, and the elastic-engineering constants are selected to identify its elastic properties (i.e., modulus of elasticity, Poisson's ratio and shear modulus).

The multiple CFRP sheets and the adhesive layers in-between which used to strengthen the CFST beams are transferred all to become one equivalent CFRP layer 'CFRP patch' in the suggested FE models,, following the same concept adopted in [15-16]. The current study assumes that all of the adhesive layers have a constant thickness, and both CFRP sheets and adhesive layers have the same width. The adhesive layer between the steel surface and the CFRP sheet is excluded from the CFRP patch because it is adopted independently in the FE model. The total thickness and the equivalent values of the ultimate tensile strength and modulus of elasticity for each CFRP patch are estimated as follows:

$$t_{cfrp.patch} = \left(n \times t_{cfrp.sheet}\right) + \left((n-1) \times t_{ad}\right) \tag{4}$$

$$\sigma_{cfrp.patch} = \left(\left(n \times t_{cfrp.sheet} \times \sigma_{cfrp.sheet}\right) + \left((n-1) \times t_{ad} \times \sigma_{ad}\right)\right) / t_{cfrp.patch} \tag{5}$$

$$E_{cfrp.patch} = \left(\left(n \times t_{cfrp.sheet} \times E_{cfrp.sheet}\right) + \left((n-1) \times t_{ad} \times E_{ad}\right)\right) / t_{cfrp.patch} \tag{6}$$

2.4.4. Adhesive

The adhesive material used in this study is MBrace saturant material supplied by BASF. This material consists of two parts with a mixing ratio of 100:40 (based on weight) (resin: hardener). The primary physical properties of this adhesive material are tensile strength, modulus of elasticity and Poisson's ratio, with value of 17 MPa, 1.138 GPa and 0.4, respectively.

The adhesive material is principally applied along the surface interaction between the CFRP patch and the steel tube surface as well as to bond the multiple layers of CFRP sheets together. However, in this study, the adhesive layer along the surface interaction between the steel and the CFRP patch is located under a mixed-mode zone of cohesive laws. The reason is that the adhesive layer is simultaneously subjected to tension (normal) and shear stresses; the failure caused by the combined stresses is known as a mixed-mode delamination. Consequently, the mixed-mode delamination combines two types of delamination modes that could occur along the cohesive surface, and this process is accurately described by [21]. The first mode, mode-I, refers to a delamination caused by pure tension (normal) stresses, whereas the second mode, mode-II, pertains to a delamination caused by pure shear stresses along the both tangential directions of the adhesive material (first and second shear directions). Several researchers have implemented the mixed-mode delamination of the adhesive material in their FE simulations and achieved accurate results compared to the results obtained by experimental works, such as [9, 16].

Figure 4 shows the stress-displacement (stress-separation) relationship used in the current study for pure mode-I and mode-II; the cohesive laws are represented as simple bilinear curves, similar as presented by De Lorenzis et al. [9]. The bilinear curves describe the stages of cohesive failure during the analysis, including the damage initiation point until the final damage. However, the stresses in both modes gradually increase relative to their displacements until they reach the point of their peak strength value (T_n and T_s). Damage starts to emerge at this stage, which is commonly known as 'damage initiation'. The curve subsequently takes another slope caused by the gradual decrease in the stresses, until the ultimate failure occurs at the final separation displacement; this stage is known as 'damage evolution'. The total area under the bi-linear curves is known as the 'interfacial fracture energy', or G_I and G_{II}, of mode-I and mode-II, respectively.

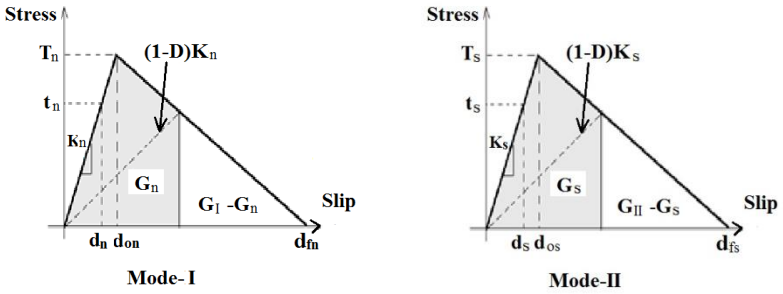

Fig. 4. Interfacial bilinear curves for pure mode-I and mode-II.

Implementing Damage Initiation

The ABAQUS software library consists of four failure criteria for implementing the 'damage initiation' of cohesive laws. These criteria are maximum nominal stress, maximum nominal strain, quadratic nominal stress, and quadratic nominal strain. The first two criteria assume that adhesive damage begins only when the maximum nominal stress or strain only reaches the capacity of the adhesive, whereas the last two criteria consider the combination effect of stresses or strains

on the damage initiation in the adhesive layer [18]. However, since the adhesive layer are subjected to combined stresses (normal and shear stresses) due to the bending loads and these stresses contribute to the adhesive failure [9]. Therefore, the mixed mode failure criterion "quadratic nominal stress", which considers both mode I and mode II failures has been selected in this study, adhesive damage is assumed to initiate based on the following equation:

$$\left\{\frac{\langle t_n \rangle}{T_n}\right\}^2 + \left\{\frac{t_s}{T_s}\right\}^2 + \left\{\frac{t_t}{T_t}\right\}^2 = 1 \tag{7}$$

The Macaulay bracket⟨ ⟩, which represents the compression stress of the adhesive material at a normal direction, is disregarded for damage initiation.

Implementing Damage Evolution

Once the damage initiation occurs, the stresses of the adhesive material start to gradually decrease until the ultimate failure (final separation) occurs, which is a stage known as 'damage evolution'. The ABAQUS software accurately represents this stage; the software is internally programmed to provide variable *D* that is introduced as a reduction factor ranging from zero to one and multiplied by the interfacial stiffness. However, *D* is equal to zero at the starting point of damage, and D is equal to one at complete failure, as shown in Fig. 4. Therefore, the following equation represents the interfacial behaviour of the reduction stresses at the damage evolution stage under a mixed-mode zone:

$$\begin{Bmatrix} t_n \\ t_s \\ t_t \end{Bmatrix} = \begin{Bmatrix} (1-D^*)K_n & 0 & 0 \\ 0 & (1-D)K_s & 0 \\ 0 & 0 & (1-D)K_t \end{Bmatrix} \times \begin{Bmatrix} d_n \\ d_s \\ d_t \end{Bmatrix} \tag{8}$$

where '*' denotes that if t_n is compressive stress, then D will be zero.

To complete the cohesive failure (final separation) under the mixed-mode delamination behaviour, the following equation of fractural energies must be satisfied in the FE software using linear power law (power-law = 1.0):

$$\frac{G_n}{G_I} + \frac{G_s}{G_{II}} + \frac{G_t}{G_{II}} = 1 \tag{9}$$

The linear elastic modulus properties for the adhesive material are required for accurately implementing the damage initiation and damage evaluation, which are known as 'elastic stiffness' or 'interfacial stiffness' for normal and both shear directions, respectively, as shown in Fig. 4. These values should be obtained from the normal and shear experimental tests of the adhesive material; however, in this study, the values are estimated based on the following concept provided by Fernando [19]:

$$K_n = E_{ad} / t_{ad} \tag{10}$$

$$K_s = K_t = 3 \times (G_{ad} / t_{ad})^{0.65} \tag{11}$$

The peak values of strength for normal (T_n) and both shear directions (T_s and T_t) are typically obtained from experimental tests and/or from material data sheet. In this study, T_n is obtained exactly as the peak strength value given in the material data sheet; nevertheless, the peak values of strength along both shear directions are assumed to be $T_s=T_t=0.9T_n$ based on the suggestion of [19].

2.5. Meshing convergence study

A convergence study is conducted for the quarter specimen of the numerical model (FE model) of the CFST beam to verify the selected meshing size for the suggested FE models. However, the maximum carrying load capacity of the FE model is compared to the maximum failure load of the experimental test conducted by [14], which is 109.0 kN for control beam (CB2). Figure 5 shows a comparison between several FE models with various numbers of elements. The FE model with the 12000 elements was selected in this study, because this model took a reasonable amount of program running time (on a normal PC) and also it's satisfied the failure load with reasonable deviation percentage which is +2.7% higher than the experimental value. In addition to that it shows better curve's behaviour when compared to the experimental model even better than the models that with 6000 elements.

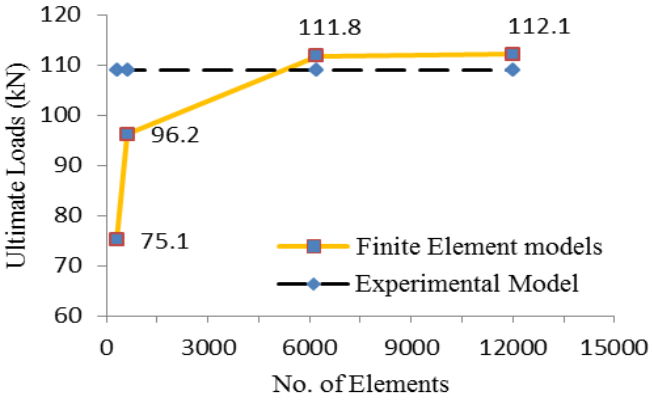

Fig. 5. Meshing convergence study.

3. Validity of Surface Interaction Techniques

To investigate the validity of the suggested surface interaction techniques (TI, CE and CB), the results of the FE models are compared to the results of the existing experimental tests of the CFST beams strengthened by CFRP sheets conducted by [14]. Sundarraja and Prabhu [14] investigated the capacity of simply supported CFST beams strengthened by CFRP sheets from the bottom side only with various wrapping scenarios (flat and U-shape). These beams mainly consisted of square hollow steel tubes and filled in by normal concrete. However, one group of beams was tested as control beams (CFST beams without CFRP sheet), whereas six groups of CFST beams were wrapped by flat strips of CFRP sheets have been considered in the present study. The second, third and fourth groups were tested with a full wrapping beam's length (FWB=100%L_n) but with different CFRP layers (1, 2 and 3, respectively). Meanwhile, the fifth, sixth and seventh groups of CFST beams were

tested with a partial wrapping length (PWB=33%L_n) with different CFRP layers (1, 2 and 3, respectively). The material properties used to build the FE models of strengthened CFST beams have been previously explained (see section 2.4).

The details of comparison between the results of tested specimens (average value for each group) and those of the FE models are listed in Table 1. The results of the maximum failure load and mid-span deflection of the beam are compared for models with each surface interaction technique independently. In general, the results of the FE models indicate an overestimation of the results conducted by the experimental works. The mean value and coefficient of variation for the failure load ratio (P_{CB}/P_{EX}) for models with the CB technique are 1.045 and 0.055, respectively, and the values for their mid-span deflection ratio (MD_{CB}/MD_{EX}) are 1.146 and 0.08, respectively. Almost close results were observed for the models with the CE technique, where the mean value and coefficient of variation for their load ratio are 1.047 and 0.059, respectively, and for their mid-span deflection ratio are 1.158 and 0.078, respectively. Meanwhile, higher deviation has been recorded for the mean value and coefficient of variation values obtained from the results of models with TI technique, where for failure load ratio (P_{TI}/P_{EX}) was 1.122 and 0.069, respectively, and for mid-span deflection ratio (MD_{TI}/MD_{EX}) a 1.487 and 0.337, respectively.

Figure 6 shows the comparison of the moment-deflection relationship between the curves of the specific experimental specimens [14] and the curves for the FE models prepared in present study for each surface interaction technique. Figure 6(a) shows the comparison between the control beams of the experimental specimen and the FE models. Figures 6(b) - (d) show the comparison between the experimental specimens and the FE models for beams with a full wrapping length (FWB=100%L_n) by 1, 2 and 3 CFRP layers, respectively. Meanwhile, Figs. 6(e)-(g) presents the comparison between the experimental specimens and FE models with a partial wrapping length (PWB=33%L_n) by 1, 2 and 3 CFRP layers, respectively. Therefore, from the above comparisons in Table 1 and Fig. 6 it can be conclude that, the FE models with the CE and CB techniques achieved perfectly the results of the experimental tests and much better than the models with TI technique. Both techniques (CE and CB) well implemented the CFRP rupture and delamination failure modes which occurred for the beams with full and partial wrapping lengths (FWB and PWB), respectively, whereas the FE models with the TI technique could be applicable for beams strengthened by CFRP sheets with a full wrapping length; the technique could not accurately implement the delamination failure, which occurred for partial wrapping beams.

Furthermore, the photos in Fig. 7 show that the delamination failure occurs on the beams with partial wrapping length (PWB) for experimental test and FE models those with CE and CB surface interaction techniques, in which both techniques (CE and CB) implement the actual delamination failure that is exactly the same failure occurred for the experimental specimen. Where, Fig. 7(a) shows the delamination failure which was occurred for specimen PWB-L1(1) test conducted by [14], and Fig. 7(b) shows the delamination failure has been occurred for CFRP sheet along the surface interaction with steel tube when the cohesive behaviour technique (CB) used for equivalent FE model W33-L1-CB. Meanwhile, Fig. 7(c) shows the deformation behaviour of adhesive material element which is provided between CFRP and steel tube elements when the cohesive elements technique (CE) used for equivalent FE model W33-L1-CE.

Table 1. Comparison the results of FE models with those obtained from the experimental tests conducted by [14].

	Experimental results (group's average value)			FE model with Tie Interaction (TI)				FE model with Cohesive Element (CE)				FE model with Cohesive Behaviour (CB)			
#FE models designations	Experimental beams designations	P_{EX} Failure Load (kN)	MD_{EX} Max. Def. (mm)	P_{TI} Failure load (kN)	MD_{TI} Max. Def. (mm)	P_{TI}/P_{EX}	MD_{TI}/MD_{EX}	P_{CE} Failure load (kN)	MD_{CE} Max. Def. (mm)	P_{CE}/P_{EX}	MD_{CE}/MD_{EX}	P_{CB} Failure load (kN)	MD_{CB} Max. Def. (mm)	P_{CB}/P_{EX}	MD_{CB}/MD_{EX}
CB	CB	108.00	63.19	112.0	69.1	1.037	1.094	112.0	69.1	1.037	1.094	112.0	69.1	1.037	1.094
W100-L1-*	FWB-L1	116.00	36.78	122.5	43.7	1.056	1.188	123.2	43.7	1.062	1.188	122.0	43.3	1.052	1.177
W100-L2-*	FWB-L2	121.33	35.25	138.1	44.1	1.138	1.251	137.9	44.2	1.137	1.255	137.2	43.9	1.131	1.245
W100-L3-*	FWB-L3	138.00	39.41	155.0	46.1	1.123	1.170	154.9	45.5	1.122	1.155	154.3	45.9	1.118	1.165
W33-L1-*	PWB-L1	108.00	33.18	116.0	45.9	1.074	1.384	110.9	38.1	1.027	1.148	110.5	37.9	1.023	1.142
W33-L2-*	PWB-L2	109.67	28.52	124.8	48.3	1.138	1.694	104.5	28.2	0.953	0.989	105.1	27.3	0.959	0.957
W33-L3-*	PWB-L3	101.67	18.69	131.0	49.1	1.289	2.628	100.6	23.9	0.990	1.279	101.3	23.2	0.996	1.242
	Mean value					1.122	1.487			1.047	1.158			1.045	1.146
	SD					0.078	0.501			0.062	0.091			0.057	0.092
	COV					0.069	0.337			0.059	0.078			0.055	0.080

Beam's numbering system adopted in the present study for FE models, as following the explained example for numbering system:

- (W100-L1) meaning this specimen of finite element beam strengthened by CFRP with full wrapping length (L_{cfrp}=100%L_n) by 1 layer of CFRP sheet.
- (W33-L3) meaning this specimen of finite element beam strengthened by CFRP with partial wrapping length (L_{cfrp}=33%L_n) by 3 layer of CFRP sheet.

* Indication for which type of surface interaction technique used for this FE models, either TI, CE or CB

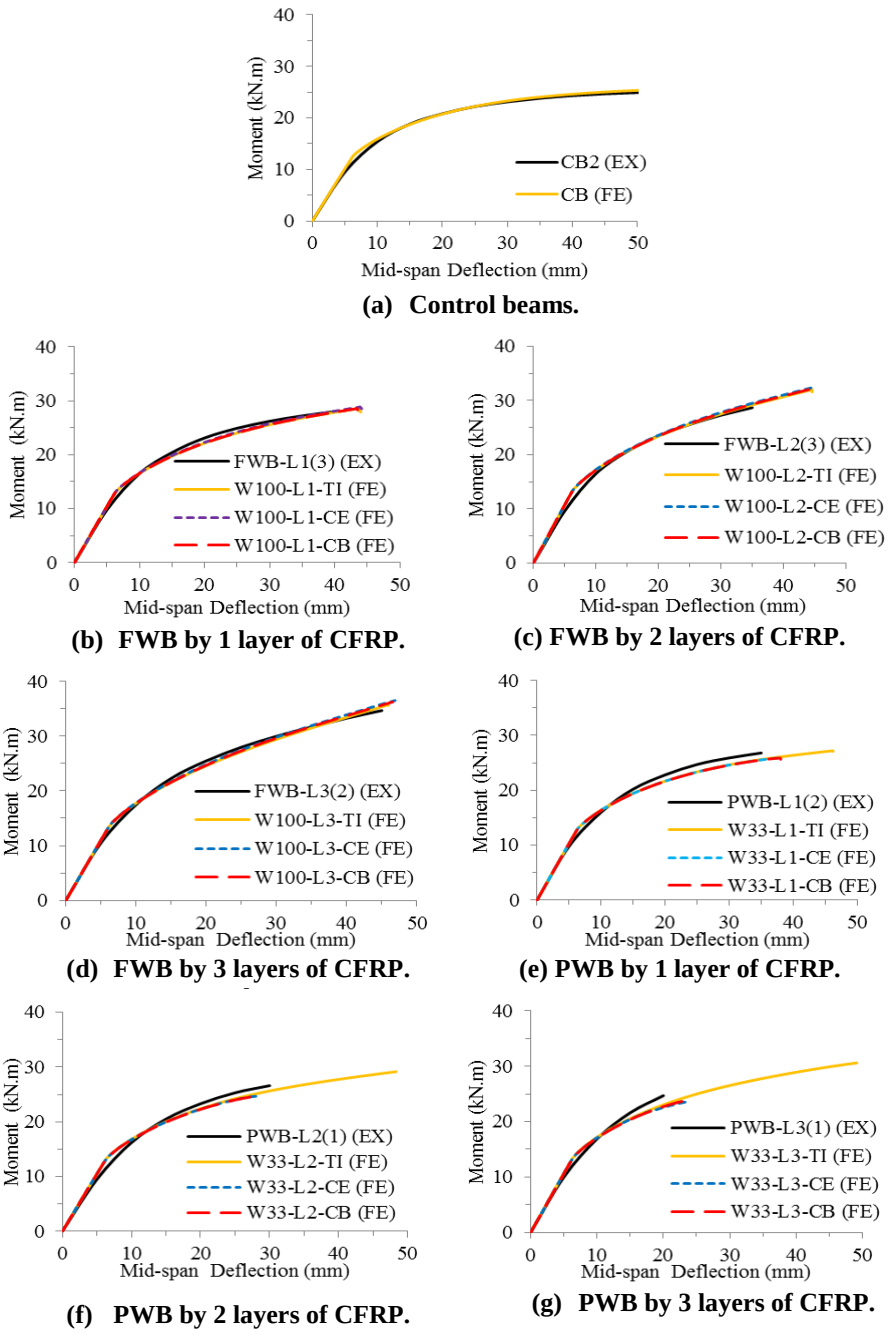

(a) Control beams.

(b) FWB by 1 layer of CFRP.

(c) FWB by 2 layers of CFRP.

(d) FWB by 3 layers of CFRP.

(e) PWB by 1 layer of CFRP.

(f) PWB by 2 layers of CFRP.

(g) PWB by 3 layers of CFRP.

Fig. 6. Comparison of the moment- deflection relationships between the experimental study [14] and the FE analysis using varied surface interaction techniques.

(a) Experimental specimen - PWB-L1(1), [14].

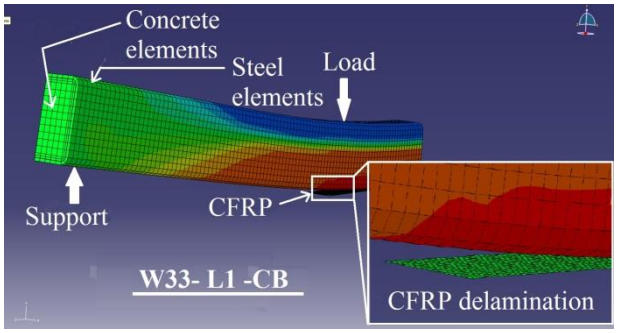

(b) Quarter FE model -W33-L1-CB.

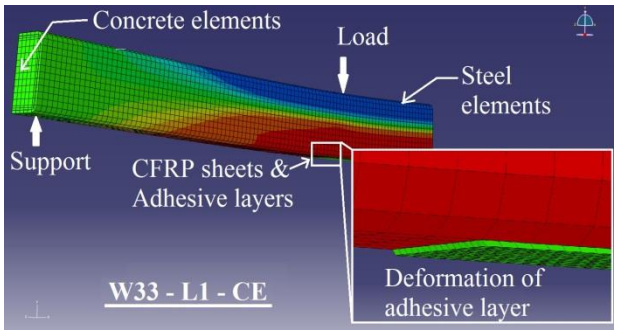

(c) Quarter FE model - W33-L1-CE.

Fig. 7. CFRP delamination failure of FE models and experimental specimen.

4. Conclusions

The conclusions of comparison between the existing experimental tests and the FE models using varied surface interaction techniques (tie interaction, cohesive element and/or cohesive behaviour) between the steel tube and the CFRP sheet, which were prepared in this study are summarized as follows:

- In general, the proposed 3D FE models effectively represent the experimental tests behaviours of CFST beams strengthened by CFRP sheets.

- FE models with a full wrapping length demonstrate a continual increase in the load capacity as the number of CFRP layers increases. Meanwhile, the models with a partial wrapping length exhibit a decrease/no further improve in the load capacity as the number of CFRP layers increases, because of the CFRP delamination failure previously occurred due to the increasing layers of CFRP sheets.
- The FE models with the TI technique effectively represent the beams with a full wrapping length only, where their CFRP sheets was totally ruptured from the mid-span once achieved its ultimate tensile strength. Meanwhile, this technique (TI) inaccurately represents the experimental specimens with a partial wrapping length because it could not implement well the CFRP delamination failure. Where, the ratios of ultimate loads and maximum deflections obtained from these FE models achieved about 1.122 and 1.487, respectively, compared to the values of the experimental tests.
- The FE models with CE and/or CB surface interaction techniques, both accurately represent the experimental beams with both strengthening scenarios (full and partial wrapping lengths). These models achieved mean values of their ultimate loads ratios approximately of 1.047 and 1.045 for the models with CE and CB techniques, respectively, compared to the values of corresponding experimental specimens, whereas their mean values of the maximum deflections ratios achieved about 1.158 and 1.148, respectively.

References

1 Nakamura, S.-I.; Momiyama, Y.; Hosaka, T. and Homma, K. (2002). New technologies of steel/concrete composite bridges. *Journal of Constructional Steel Research*, 58(1), 99-130.

2 Zhao, X.-L.; and Zhang, L. (2007). State-of-the-art review on FRP strengthened steel structures. *Engineering Structures*, 29(8), 1808-1823.

3 El Damatty, A.A.; and Abushagur, M. (2003). Testing and modeling of shear and peel behavior for bonded steel/FRP connections. *Thin-Walled Structures*, 41 (11), 987-1003.

4 Al-Emrani, M.; Linghoff D.; and Kliger, R. (2005). Bonding strength and fracture mechanisms in composite steel-CFRP elements. *Proceedings of the International Symposium on Bond Behaviour of FRP in Structures (BBFS 2005)*, International Institute for FRP in Construction, Canada, 425-433

5 Fawzia, S.; Zhao, X.L.; Al-Mahaidi, R., and Rizkalla, S. (2005). Bond characteristics between cfrp and steel plates in double strap joints. *Advanced Steel Construction*, 1(2), 17-27.

6 Al-Zubaidy, H.; Al-Mahaidi, R.; and Zhao, X.-L. (2012). Experimental investigation of bond characteristics between CFRP fabrics and steel plate joints under impact tensile loads. *Composite Structures*, 94(2), 510-518.

7 Yang, J.Q.; Smith, S.T.; and Feng P. (2013). Effect of FRP-to-steel bonded joint configuration on interfacial stresses: Finite element investigation. *Thin-Walled Structures*, 62, 215-228.

8 Campilho, R.D.S.G.; de Mour, M.F.S.F.; and Domingues, J.J.M.S. (2008). Using a cohesive damage model to predict the tensile behaviour of CFRP

single-strap repairs. *International Journal of Solids and Structures*, 45(5), 1497-1512.

9 De Lorenzis, L.; Fernando, D.; and Teng, J.-G. (2013). Coupled mixed-mode cohesive zone modeling of interfacial debonding in simply supported plated beams. *International Journal of Solids and Structures*, 50(14-15), 2477-2494.

10 De Lorenzis, L.; and Zavarise, G. (2009). Cohesive zone modeling of interfacial stresses in plated beams. *International Journal of Solids and Structures*, 46(24), 4181-4191.

11 Tao, Z.; and Han, L.-H. (2007). Behaviour of fire-exposed concrete-filled steel tubular beam columns repaired with CFRP wraps. *Thin-Walled Structures*, 45(1), 63-76.

12 Haedir J.; Bambach M.R.; Zhao X.L.; and R.H. Grzebieta (2009). Strength of circular hollow sections (CHS) tubular beams externally reinforced by carbon FRP sheets in pure bending. *Thin-Walled Structures*, 47(10),1136-1147.

13 Haedir, J.; Zhao, X.-L.; Grzebieta, R.H.; and Bambach, M.R. (2011). Non-linear analysis to predict the moment–curvature response of CFRP-strengthened steel CHS tubular beams. *Thin-Walled Structures*, 49(8), 997-1006.

14 Sundarraja, M.C.; and Prabhu, G.G. (2013). Flexural behaviour of CFST members strengthened using CFRP composites. *Steel and Composite Structures*, 15(6), 623-643.

15 Fawzia, S.; Al-Mahaidi, R.; and Zhao, X.L. (2006). Experimental and finite element analysis of a double strap joint between steel plates and normal modulus CFRP. *Composite Structures*, 75(1-4), 156-162.

16 Al-Zubaidy, H.; Al-Mahaidi, R.; and Zhao, X.L. (2013). Finite element modelling of CFRP/steel double strap joints subjected to dynamic tensile loadings. *Composite Structures*, 99, 48-61.

17 Nishikawa, M.; Okabe, T.; and Takeda, N. (2007). Numerical simulation of interlaminar damage propagation in CFRP cross-ply laminates under transverse loading. *International Journal of Solids and Structures*, 44(10),3101-3113.

18 ABAQUS, Documentation Version 6.8, 2008: Hibbit, Karlson and Sorensen, Inc., USA.

19 Fernando, N.D. (2010). *Bond behaviour and debonding failures in CFRP-strengthened steel members*. PhD Thesis, Civil and structural department, Hong Kong Polytechnic University, Hong Kong, China.

20 Byfield, M.P.; Davies, J.M.; and Dhanalakshmi, M. (2005). Calculation of the strain hardening behaviour of steel structures based on mill tests. *Journal of Constructional Steel Research*, 61(2), 133-150.

21 Camanho, P.P.; and Dávila, C.G. (2002). Mixed-mode decohesion finite elements for the simulation of delamination in composite materials. *Technical paper 211737(1)*, 33, NASA, USA.